We are IntechOpen, the world's leading publisher of Open Access books Built by scientists, for scientists

6,900
Open access books available

185,000
International authors and editors

200M
Downloads

Our authors are among the

154
Countries delivered to

TOP 1%
most cited scientists

12.2%
Contributors from top 500 universities



WEB OF SCIENCE™

Selection of our books indexed in the Book Citation Index in Web of Science™ Core Collection (BKCI)

Interested in publishing with us?
Contact book.department@intechopen.com

Numbers displayed above are based on latest data collected.
For more information visit www.intechopen.com



26

Facts about Producer Gas Engine

G. Sridhar[1] and Ravindra Babu Yarasu[2]
[1]*Siemens Corporate Research and Technologies, Bangalore,*
[2]*Govt. College of Engineering, Amravati, Maharashtra,*
India

1. Introduction

Reciprocating internal combustion engines have integrated into society service since the middle of 20th century. Their use has improved the quality of life substantially, but at the cost of degradation to the environment as well as depletion of fossil fuels, certainly due to insufficient environmental consciousness in several countries. Therefore, large impetus is being given to reduce the emissions by two approaches namely, increasing the engine efficiency and the use of alternate fuels in place of fossil fuels. In present chapter, the use of alternate fuels has been addressed along with modeling and simulation of engine combustion.
In the domain of alternative fuels, gaseous fuels receive more prominence because of the possibility of cleaner combustion. Among the gaseous fuels, producer gas derived from biomass gasification is a better option as an environment friendly fuel. This fuel gas, in addition to being CO_2 neutral, generates lesser quantity of undesirable emissions. Even though the merits of producer gas have been recognized earlier, the technological capitalization has remained in infancy.
The thermo-chemical conversion of biomass leads to generation of a gas generally termed as producer gas. The process is termed as gasification implies that a solid fuel is converted to a gaseous fuel. Gasification is not a new technology but is known ever since World War II. During this period a number of vehicles in Europe were powered with charcoal gasifiers (ANON-FAO Report, 1986). It is estimated that over seven million vehicles in Europe, Australia, South America and Pacific Islands were converted to run on producer gas during World War II. These engines were spark ignition (SI) engines, mostly operating in the lower compression ratio (CR) range and based either on charcoal or biomass derived gas.
At the far end of 20th century, there was a renewed interest in biomass gasification technology, which had stimulated interest in producer gas operated engines. Prior to 21st century, the work reported in this area had been limited to lower CR (less than 12.0) engine due to perceived limitation of knock at higher CR. A short review of some of earlier studies, related to producer gas engine is presented in the following section in order to explain the context for this topic.

2. Literature review

Literature survey in the field of producer gas based engines reveals modest research work to have been carried out since the inception of biomass/charcoal gasification systems. This

could be attributed to two reasons, namely non-availability of standard gasification system that could generate consistent quality producer gas and the other relating to misconceptions about producer gas fuel.

It was reported that Europe exploited the most of gasification technology during petroleum oil crisis of World War II. Among the European nations, Sweden accounts for a large amount of work in the area of wood and charcoal gasification. National Swedish Testing Institute of Agricultural Machinery, Sweden (ANON-FAO Report, 1986) has reported extensive work on the design and development of closed top charcoal and wood gasifiers for use with the reciprocating engines. These engines were however in the lower compression ratio (CR) – 10, either adapted from petrol engines or modified diesel engine. Martin et al., (1981) reported work using charcoal gas and biomass based producer gas on a SI engine with a de-rating of 50% and 40% respectively at a CR of 7. They also claimed 20% de-rating when worked with producer gas at a CR of 11. They indicate an upper limit of CR of 14 and 11 for charcoal and biomass based producer gas, respectively.

American sub-continent also claims experimental work relating to producer gas engines. Tatom et al., (1976) reported work on a gasoline truck engine with a simulated pyrolysis gas at a de-rating of 60-65%. It was also emphasized that that the optimum ignition timing is a function of engine speed. Parke et al., (1981) worked on both naturally aspirated and super charged gas engines. The de-rating of 34% was claimed compared to gasoline operation and a lesser de-rating in a supercharged mode.

In the Indian sub-continent, work in the area of producer gas engine has been reported by the biomass gasification group of Indian Institute of Technology, Mumbai. They have reported work on a gas engine converted from a naturally aspirated diesel engine at CR of 11.5 (Shashikantha et al. 1993, 1999; Parikh et al. 1995). The reason given for limiting the CR was knocking tendency. However, no experimental evidence was provided in support of it.

If one were to summarize the findings of earlier studies (prior to 2000), it becomes evident that no systematic investigation had been attempted in identifying the existence of knock limitation, if any, with producer gas operation at CR comparable to that of diesel engine operation. On the contrary producer gas with large fraction of inert (> 50%) and with laminar burning velocity being high (due to the presence of H_2), smooth operation at higher CR must be definitely possible.

A systematic investigation on producer gas operation at CR comparable to that of diesel engine was carried out and reported by one of the present authors (Sridhar et al., 2001; Sridhar, 2003; Sridhar et al., 2006). The source of producer gas fuel used was from an open top re-burn down draft gasifier system (Mukunda et al., 1993 & 1994) using Casuarina wood pieces as the fuel. The compression ratio limits were tested up to 17:1 without any audible knocking. It was demonstrated that the comparable power to that of diesel engine (with a lesser extent of de-rating ~ 15-20%) could be achieved with producer gas by operating engine at higher CR. The outcome of the experimental work along with simulation tools to predict the engine performance is explained in the following sections.

3. Scope of the chapter

Based on the review of the published work (prior to 2000), there is no positive evidence for the presence of knock with producer gas fuel in spark ignition (SI) engines at higher CR than 14. This restriction in compression ratio (CR) was simply a matter of presumption rather

than fact. One of the primary objectives of this chapter is to present the results of producer gas based SI engine operating at the higher possible CR. The results of a systematic investigation, which includes the in-cylinder pressure measurements are presented. Assessing the thermodynamic behaviour of the engine, nitric oxide emissions and also validation of the engine simulation models with help of the measured in-cylinder pressure data are discussed.

The in-cylinder processes in a reciprocating engine are extremely complex in nature. While much is known about these processes, they are not adequately understood at a fundamental level, especially the combustion process. Tools used for prediction of in-cylinder processes in a reciprocating engine operating on producer gas are mentioned. The comparisons of results of two different combustion models against experimental data are presented. A Zero-dimensional thermodynamic model can give quick results. However, it fails to predict the results accurately at wide range of varied ignition timings. It is due to the varying degree of favorable or adverse effect of reverse squish flow on burning of mixture inside the cylinder, particularly at high CR. Whereas a multi-dimensional combustion model, based on Flame surface density can give a better prediction of engine performance. The objective of including the engine simulation work is to predict the burn rate in a producer gas fuelled SI engine under the influence of varying ignition timing and compression ratio.

The first model, i.e., a Zero-dimensional model was used to simulate the complete thermodynamic cycle. Eddy entrainment and laminar burn-up (EELB) postulated by Keck (1982), was adopted to compute burn rate with parameters of turbulence properly accounted for engine geometry under study. A curve fit equation of laminar burning velocity of Producer gas at pressures and temperature relevant to engine operation is presented which can be used in combustion simulation models. The second model, based on Flame surface density, for multi-dimensional combustion simulation was used with wall correction. The limitations and capabilities of these models are explained.

4. Properties of Producer gas

Some of the fundamental data relating to producer gas along with pure gases is given in Table 1. The comparison of producer gas with methane is more vital with regard to the internal combustion engine operation. This is because most of the engines operating on gaseous fuels are either close to pure methane (natural gas) or diluted methane (bio-gas, land-fill gas). The fuel-air mass equivalence ratio, i.e., (actual fuel to air ratio)/(stoichiometric fuel to air ratio) at the flammability limits compares closely for both the gases, but the laminar burning velocity for producer gas at the lean limits is much higher. The laminar burning velocity for producer gas (at 0.1MPa, 300K) is about 0.5 m/sec which is about 30% higher than methane. This feature demand lower advancement in the ignition timing for the engine based on producer gas fuel.

Like any other gaseous fuel, producer gas can be used for internal combustion engine operation provided that the gas is sufficiently clean and contaminant does not accumulate in the intermediary passages to the engine cylinder. But this fuel has largely been left unexploited due to additional perceptions, namely (1) auto-ignition tendency at higher CR, (2) large de-rating in power due to lower calorific value. However, these perceptions were re-examined (Sridhar et al., 2001). Firstly, as the laminar burning velocity being high due to the presence of hydrogen (more so, with the gasifier system adapted) might reduce the tendency for the knock. Secondly, the presence of inert in the raw gas (CO_2 and N_2) might

suppress the pre-flame reactions that are responsible for knocking on account of increased dilution. Also the maximum flame temperature attainable with the producer gas being lower compared to conventional fuels like methane, one could expect better knock resistivity.

Furthermore, there is a general perception that producer gas being a low-energy density fuel, the extent of de-rating in power would be large when compared to high- energy density fuels like natural gas and Liquefied petroleum gas. This could be misleading because what needs to be accounted for comparison is the charge mixture energy density (Fleischer et al., 1981) and not the fuel energy density *per se*. On comparison with CH_4, the mixture energy density for producer gas is lower by 23% as reflected in Table 1. The product to reactant mole ratio for producer gas is less than one. These two parameters could contribute to de-rating of engine output. However, it might be possible to reduce de-rating by working with engines of higher CR, perhaps higher than what has been examined using natural gas at CR=15.8 (Das & Watson, 1997).

Fuel + Air	Fuel LCV, MJ/kg	Air/Fuel @ (Φ =1)	Mixture, MJ/kg	Φ, Limit		S_L (Limit), cm/s		S_L Φ =1, cm/s	Peak Flame Temp, K	Product/ Reactant Mole Ratio
				Lean	Rich	Lean	Rich			
H_2	121	34.4	3.41	0.01	7.17	65	75	270	2400	0.67
CO	10.2	2.46	2.92	0.34	6.80	12	23	45	2400	0.67
CH_4	50.2	17.2	2.76	0.54	1.69	2.5	14	35	2210	1.00
C_3H_8	46.5	15.6	2.80	0.52	2.26	-	-	44	2250	1.17
C_4H_{10}	45.5	15.4	2.77	0.59	2.63	-	-	44	2250	1.20
PG	5.00	1.35	2.12	0.47 a	1.60 b	10.3	12	50 c	1800 d	0.87

PG: H_2 - 20%, CO - 20%, CH_4 - 2%; a: $\pm$0.01, b: $\pm$0.05, c: $\pm$5.0, d: $\pm$50 ; LCV: Lower Calorific Value

Table 1. Properties of Producer Gas (PG) Compared with Pure Combustible Gases

4.1 Laminar burning velocity (S_L) of Producer gas

The laminar combustion properties of gaseous fuels at high temperatures and pressures are of fundamental importance for analyzing and predicting the performance of internal combustion engines and power plant burners. Experimental laminar burning velocity can also be used to check theoretical combustion models and calculate apparent activation energies.

Laminar burning velocity (S_L) of a gaseous fuel is function of reactant mixture pressure and temperature. For Producer gas, Laminar burning velocity is also function of its composition. To establish the S_L values of producer gas, efforts were made by few researchers at ambient and higher pressure and temperature conditions. Experimental and theoretical calculation works made by the researchers to determine the laminar burning velocity of producer gas-air mixtures are presented below.

Kanitkar et al., (1993) determined the laminar flame speed (S_L) at ambient conditions (0.96 bar, 300 K) by conducting experiments using flame tube apparatus for producer gas-air mixture. These experiments were conducted at laboratory reference conditions using producer gas generated from IISc's on-line open top re-burn gasification system. The gas

consisted of 18-23% H_2, 17-20% CO, 3-4% CH_4, 13-14% CO_2 and rest N_2. A wide range of mixture ratios were considered within the flammability limits of rich and lean mixtures, namely equivalence ratio from 0.47 (26% fuel on volume basis) to 1.65 (56% fuel) for lean and rich limits, respectively. The physical values of burning velocity varied from 0.10 and 0.13 ms^{-1} at lean and rich limits, to the peak value of 0.50±0.05 ms^{-1} around stoichiometry (45% fuel).

Experimental laminar burning velocity (S_L) values of producer gas at high pressures and temperatures were reported by Keshavamurthy et al., (2004). The experiments were conducted in a spherical combustion vessel. Synthetic mixtures of producer gas with a composition of 22% H_2, 22% CO, 4% CH_4, 10% CO_2 and 42% N_2 were used to determine S_L at initial pressures of 0.5 to 5 bar and ambient temperature. With these initial pressures and temperature a peak pressure of 30 bar during combustion and a maximum unburnt gas temperature of 450 K were obtained. The unburnt gas temperatures were obtained by assuming isentropic compression of unburnt gases as the combustion progresses. The experiments were conducted at equivalence ratios (ratio of actual fuel-air mass ratio to the stoichiometric fuel-air mass ratio) in the range of 0.8 to 1.4. The laminar burning velocity values have been deduced from the pressure-time measurements. The variation of S_L values with respect to pressure, temperature and equivalence ratio was presented. The experimental data points were fitted with a power law equation of the form $S_L = aP^b$ where a and b were curve fit coefficients. Different sets of a and b values for different initial temperatures were specified. The burning velocity values were extrapolated from higher pressures and temperatures to ambient conditions to arrive at a value of 0.47 ms^{-1} at stoichiometric conditions.

Sridhar et al. (2005) reported computational results concerning the laminar burning velocity of a biomass-derived producer gas and air mixture at pressures and temperatures typical of the unburned mixture in a reciprocating engine. Based on a number of calculations at varying pressures (5-50 bar) and temperatures (630-1082 K), and equivalence ratios (0.9-1.07), an expression for estimating the laminar burning velocity with the residual gas (RG) mass fraction (0-10%) was obtained. Also, the effects of varying residual gas in the engine cylinder, H_2 and CO mass fraction in the fuel on S_L were estimated. This work on S_L is useful in predicting the burn rate in a spark ignition engines fuelled with a producer gas. The expression for estimating the laminar burning velocity, S_L in (cm/s) is as follows.

$$S_L(\text{cm/s}) = \left(\frac{p}{p_0}\right)^{0.2744} 94.35\ \big(0.96 + 1.2(\Phi - 1)\big)(1 - 2.4\psi) \quad (1)$$

where p is the pressure of the mixture in engine cylinder in kPa, p_0 is the reference pressure, i.e., 100 kPa, Φ is the equivalence ratio of the mixture, Ψ is the residual gas (RG) mass fraction in the engine cylinder. The burning velocity dependence upon the initial temperature is built into the pressure term in Eq. (1).

Natarajan et al., (2007) reported laminar flame speeds of lean $H_2/CO/CO_2$ (syngas) fuel mixtures, which have been measured over a range of fuel compositions (5-95% for H_2 and CO and up to 40% for CO_2 by volume), reactants preheat temperatures (up to 700 K), and pressures (1-5 atm). Two measurement approaches were employed: one using flame area images of a conical Bunsen flame and the other based on velocity profile measurements in a

one-dimensional stagnation flame. These data were compared to numerical flame speed predictions based on two established chemical mechanisms: GRI Mech 3.0 and the Davis H_2/CO mechanism with detailed transport properties. For room temperature reactants, the Davis mechanism predicted the measured flame speeds for the H_2/CO mixtures with and without CO_2 dilution more accurately than the GRI mechanism, especially for high H_2 content compositions. This work was more about the checking ability of mechanism to predict the S_L values of Syngas.

Ratnakishore et al., (2008) reported the laminar burning velocity values of producer gas from computations of spherical outwardly propagating flames and planar flames. Different reaction mechanisms were assessed for the prediction of laminar burning velocities of CH_4, H_2, H_2-CO, and CO-CH_4 and results showed that the Warnatz reaction mechanism with C1 chemistry was the smallest among the tested mechanisms with reasonably accurate predictions for all fuels at 1 bar, 300 K. Unstable flames due to preferential diffusion effects were observed for lean mixtures of fuel with high hydrogen content. On accounting the Soret effect, the variation in burning velocity was at least 5% even with 5% of hydrogen (by volume) in the binary fuel of H_2-CO.

5. Engine experimental results at varied compression ratios

Experimental results of a systematic investigation on producer gas operated internal combustion engine at higher compression ratio (CR) for the first time was reported by Sridhar et al., (2001). The primary investigation was conducted on an engine of 24 kW capacity. Experiments were conducted on a spark ignition (SI) engine converted from a naturally aspirated, three-cylinder, direct injection diesel engine (RB 33 model) of compression ratio (CR) 17. The knock sensitivity identifies the Highest Useful Compression Ratio (HUCR) for most of the fuels having higher octane number. For higher-octane fuels, it has been experimentally established that the upper limit of CR is 17 beyond which there is a fall in efficiency (Caris & Nelson, 1959).

The salient features of the diesel engine chosen for conversion to SI engine are shown in Table 2. The naturally aspirated engine of 3.3 litre capacity is designed at a CR =17, to operate at an air-to-fuel ratio of 20 - 21 (with diesel) at rated conditions. The combustion chamber of the engine is formed of a flat cylinder head and slightly offset bowl-in piston as shown in Fig.1. The bowl is hemispherical in shape and has a squish area of 70% (percentage of piston area closely approaching the cylinder head). The engine was characterized using diesel fuel prior to conversion. The trial result database obtained was consisting of in-cylinder pressure, and the specific fuel consumption at the rated speed of 1500 rev/min. The engine delivered a peak power of 21 kWe, which is equivalent to a net brake (shaft) output of 24.0 kW against the rated output of 28.0 kW (at sea level). The loss in power is attributed to lower air density at Bangalore, due to its elevation (~1000 m above sea level).

The diesel engine was modified to work as SI engine by insertion of spark plug in place of fuel injector and adapting distributor type battery based ignition system. However, the combustion chamber was left unchanged. The combustion chamber comprised of a flat cylinder head and slightly offset bowl-in-piston was retained (Fig. 1). The compression ratio was varied (17, 14.5, 13.5 and 11.5) by changing the thickness of cylinder head gasket, thereby altering the clearance volume.

Parameter	Specification
Make and Model	Kirloskar, RB-33 Coupled to a 25kVA Alternator
Engine Type	In-Line, 3 Cylinder, 4-Stroke, Naturally Aspirated
Rated Output - Diesel	28 kW @ 1500 rev/min
Net Output - Diesel	24 kW (21kWe) @ 1500 rev/min
Type of Cooling	Water Cooled with Radiator
Bore x Stroke	110 x 116 mm
Swept Volume	1.1 Litre
Compression Ratio	17:1
Bumping Clearance	1.5 mm
Combustion Chamber	Flat Cylinder Head and Hemispherical Bowl-in Piston Type
Squish Area	70%

Table 2. Engine Configuration Details

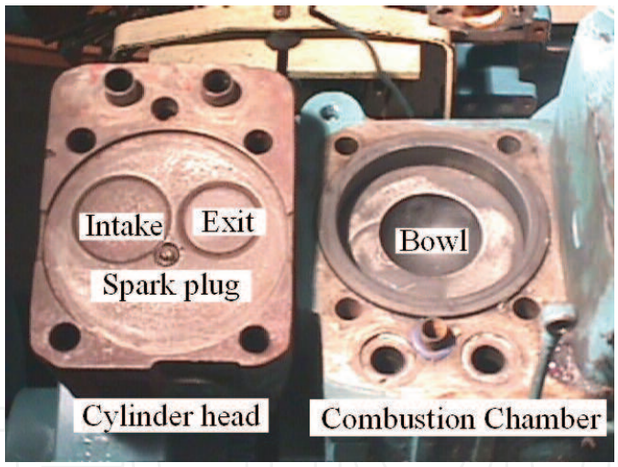


Fig. 1. Engine's combustion chamber

5.1 Instrumentation on the engine

Fig. 2 depicts the instrumentation scheme adopted for the experiments. For combustion diagnostics, the in-cylinder pressure was measured using a Piezo sensor (PCB make) mounted on the cylinder No. 1 of the engine. The sensor is hermitically sealed (model No. HS 111A22) with a built-in charge amplifier, the other specifications being: resolution - 0.69 kPa, rise time < 1 micro second, discharge time constant > 500 second, natural frequency of the crystal = 550 kHz. The in-cylinder pressure measurement synchronized with the crank angle measurement (sensed using an optical sensor) was acquired on a PC (Personal Computer, 600 MHz processor) at time intervals of one-degree crank angle.

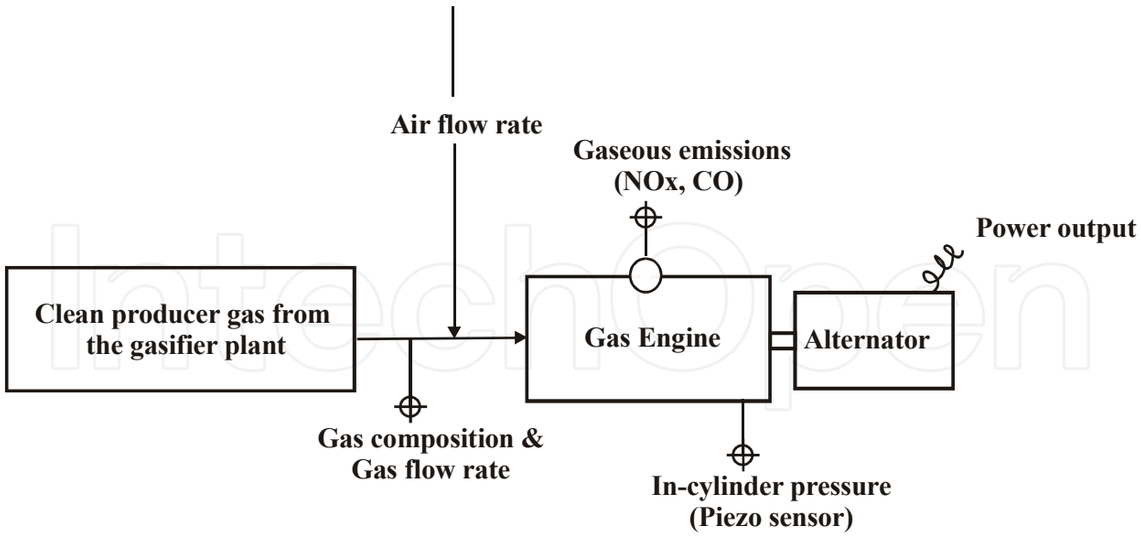


Fig. 2. Scheme for instrumentation

5.2 Engine's performance

The power developed and other important performance parameters of an engine operating on biomass generated producer gas at varied compression ratio results are presented below.

5.2.1 Power and efficiency

The first and the foremost result of these tests is that the engine worked smoothly without any sign of knock at the CR of 17. There was no sign of audible knock during the entire load range. Moreover, the absence of knock is clear from the pressure-crank angle (p-θ), which does not show any pressure oscillations, either at part load or at full load (wide open throttle) conditions. A comparison of normal and abnormal (due to knock) combustion is shown in Fig. 3. The normal performance (without pressure oscillations) shown as (i) and (ii) in Fig. 3 (a) corresponds to two firing cycles at ignition advance of 26° and 12° BTC respectively. These correspond to operations with producer gas on the converted gas engine

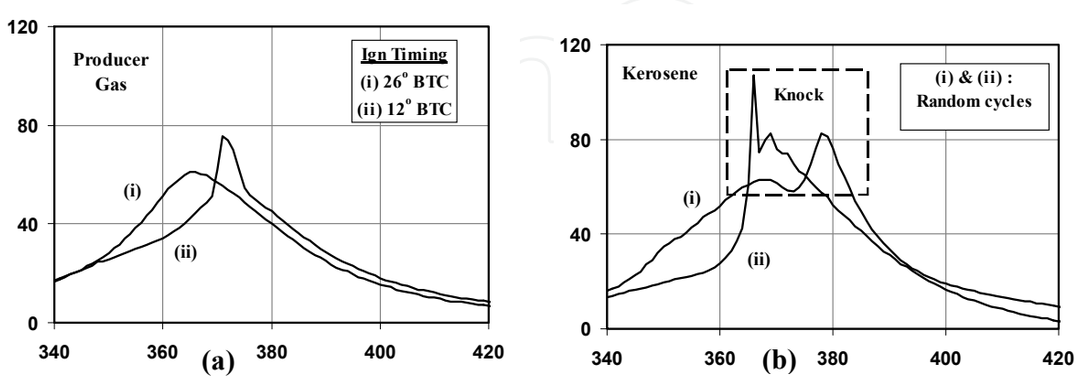


Fig. 3. (a) Normal combustion under wide open throttle condition with Producer Gas at different ignition timings at CR=17, (b) Incipient knock with Kerosene at No-Load condition with ignition timing of 30° BTC at CR=16.5.

at CR=17 under wide open throttle conditions. Whereas, performance with incipient knock (with pressure oscillations) shown as (i) and (ii) in Fig. 3 (b) corresponds to two random firing cycles. These correspond to operations with kerosene fuel on a single cylinder SI engine (converted from a diesel engine) at CR=16.5 under no-load conditions. The piezo sensor employed for p-θ recording was the same in either case.

The results of the power output with producer gas are shown in Table 3. At CR=17, the engine delivered a maximum net brake output of 20 kW (17.5 kWe) at an efficiency of 30.7% compared to 24 kW (21 kWe) brake output at 33% efficiency with diesel (compression ignition mode). The efficiency calculation is based on the ratio of net brake output to the energy content of the air and gas mixture (gas-to-shaft power). The useful output and efficiency decreased with the lowering of CR. A maximum net brake output of 17.6 kW (15.3 kWe) at an efficiency of 27.5% was obtained at CR of 11.5. The power output at intermediate CR of 14.5and 13.5 were 18.8 and 18.6 kW respectively and with efficiencies around 29%. The efficiency at CR = 13.5 was comparable to that at 14.5 probably due to relatively leaner operation. The extent of de-rating in brake power was about 16.7% at CR = 17 and increased to as high as 26% at CR = 11.5 compared with baseline operations in diesel mode.

CR	IGN, BTC	Φ	Net Elec. Power, kWe	Net Brake Power (BP_{Net}) , kW	Mixture Energy Density, MJ/kg	Efficiency : Gas-to-Shaft, %
17.0	06	1.10	17.5	20.0	2.20	30.7
14.5	10	1.10	16.4	18.8	2.20	29.0
13.5	14	1.06	16.2	18.6	2.10	29.3
11.5	15, 17	1.07	15.3	17.6	2.20	27.5

Φ =Equivalence Ratio: (Actual fuel- to- air ratio)/(Stoichiometric fuel- to- air ratio)

Table 3. Maximum net engine output at varying CR

IGN, BTC	Φ	BP_{net}, kW*	η, %	IGN, BTC	Φ	BP_{net}, kW*	η, %
CR=17.0				**CR=14.5**			
06	1.10	20.0	30.8	08	1.20	18.6	25.0
12	1.00	19.8	31.0	10	1.10	18.8	29.0
17	1.09	18.4	29.0	16	1.11	17.9	27.5
22	1.03	17.9	28.0	20	1.11	17.7	27.2
26	1.10	16.2	25.3				
33	1.25	14.0	19.0				
CR=13.5				**CR=11.5**			
08	1.05	18.2	28.6	06	1.07	17.0	27.0
14	1.06	18.6	29.0	15,17	1.07	17.6	27.5
18	1.07	17.0	27.8	27	1.09	15.6	25.5
25	1.06	17.0	28.0	38	1.07	13.3	20.0

* Excluding Radiator Fan Power

Table 4. Maximum net engine output as a function of ignition timing at varying CR

The net brake output with producer gas at varying ignition timing for the four different CRs tested is shown in Table 4. It is evident from the above data that ignition timing had to be retarded with the increase in CR in order to obtain higher output. This is because the thermodynamic conditions in terms of pressures and temperature are more severe at higher CR and thereof the combustion is faster thus calling for the optimum ignition timing to be located close to TC. The maximum output was recorded at an ignition advance of 6° BTC at CR=17 and increased to about 15 - 17° BTC at a CR=11.5. At intermediate CR of 14.5 and 13.5 the ignition advance was 10 and 14° BTC respectively. The fuel-air equivalence ratio was about 1.06 $\pm$ 0.5 in most of the cases, with efficiency of 30.7 and 27.5% corresponding to maximum output at higher and lower CRs respectively (Sridhar et al., 2001).
The incremental gain in maximum power and efficiency per unit CR is well within the range quoted in literature. The gain in power was between 2.2 and 2.6 per unit CR, but the gain in efficiency was marginally lower. However, these figures are well within the range of 1 to 3% gain per unit increment of CR reported by Heywood (1988).

5.2.2 In-Cylinder pressure measurements

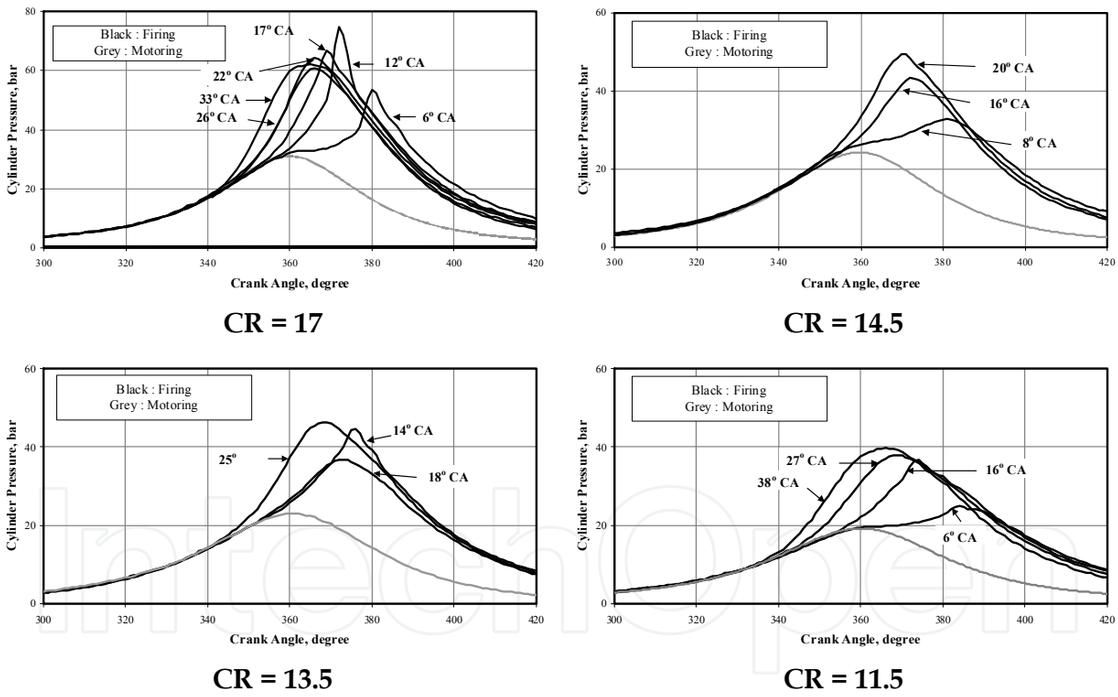


Fig. 4. p-θ Recording corresponding to maximum brake output at different ignition advance and varying CRs. (Ensemble-averaged data over 30 consecutive cycles)

The pressure-crank angle (p-θ) recording is shown in Fig. 4 at different CRs, none of these show any trace of knock for all ranges of load inclusive of peak. These figures contain ensemble average data over thirty consecutive cycles. It is clear from these curves that smooth and normal combustion seemed to occur even at advanced ignition timing of 33° CA corresponding to CR of 17. Faster burn rate due to presence of hydrogen in the fuel gas could be the principal factor for the no-knock performance. The effect of the ignition

advance on the pressure history is evident from the above curves. There are substantial differences in the maximum cylinder pressure and their point of occurrence. The ratio of maximum cylinder pressure between the highest and the lowest CR at corresponding ignition timing is about 2.

The net work delivered over a complete cycle can be found by integrating the pressure-volume (p-v) data over the four processes. This had also helped in identifying the optimum ignition timing for a given CR - commonly referred as MBT (Maximum Brake Torque). The net indicated mean effective pressure (IMEP) obtained from the integrated p-v data is a measure of effectiveness with which an engine of a given volumetric displacement converts the input energy into useful work. The IMEP obtained from ensemble average p-v data (~ 30 cycles) at varying CR as a function of ignition timing is shown in Figure 5. At CR=17, the maximum IMEP recorded is 5.98 bar corresponding to a ignition timing of 6° CA and this declined to 4.85 bar with ignition timing being 15° CA at CR of 11.5. These values are obtained at $\Phi = 1.08 \pm 0.2$ and fall within the anticipated value of $\Phi = 1.0$ to 1.1 (Heywood, 1988). It is also evident from the plot that variations in the IMEP values are modest between ignition timings of 6 and 12° CA corresponding to CR=17.

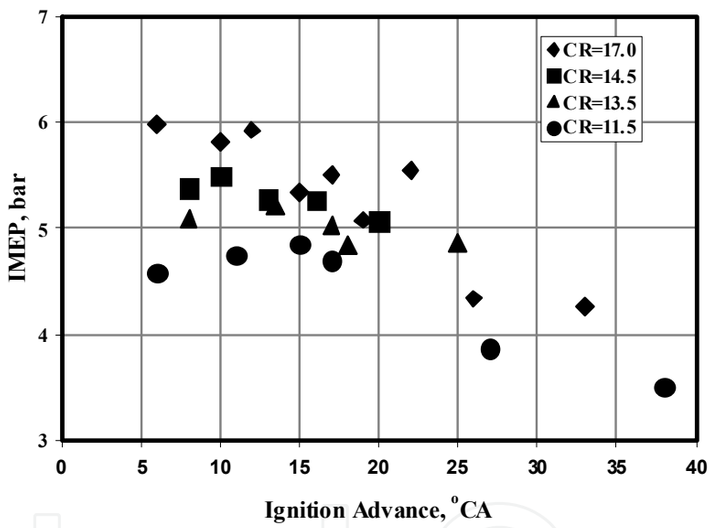


Fig. 5. Variation of IMEP (Net) with ignition advance at various CRs

Exploring further the p-θ data, the peak pressure and the point of occurrence at ignition timings close to MBT are listed in Table 5. These measurements are accurate within – 1.0° CA (due to possible lag in the signal and error in TC identification). The coefficient of variation of the IMEP at all CRs and ignition settings occurred well within 3-3.5%, implying low cycle-to-cycle variation. The reason for low cyclic variation is the faster rate of combustion occurring inside the engine cylinder. The faster rate of combustion is attributed to higher flame speeds due to the presence of hydrogen in the gas and also to the combustion chamber design.

5.2.3 Nitric oxide emission from the engine

The Nitric oxide (NO) emission from the engine was measured. The variation of NO in gas mode at varying CR with ignition advance is shown in Fig. 6. The NO level reduced with

CR	Ign. Advance, ° CA	Peak pressure, bar	Occurrence, ° ATC
17.0	6	55.00	20
14.5	10	43.30	19
13.5	14	45.00	17
11.5	15, 17	33.00, 38.00	17, 12

Table 5. Cylinder Peak Pressures and Their Occurrence

the retardation of ignition timing and this feature is observed for all CRs. The NO level is observed to be maximum at the highest CR with advanced ignition timings, whereas in the MBT range of 6 to 20° BTC the NO is lower and comparable in almost all the cases. It is well known that NO generation is strongly dependent on the temperature, oxygen availability and residence time in the combustion chamber. With the flame speed of the gas mixture being high, the ignition setting is retarded whereby the residence time in the high temperature combustion chamber is automatically reduced. Therefore the low NO levels at retarded ignition setting are an expected and consistent behavior. The above results match well with those quoted by Heywood [1988], which shows small to modest variation of NO with CR.

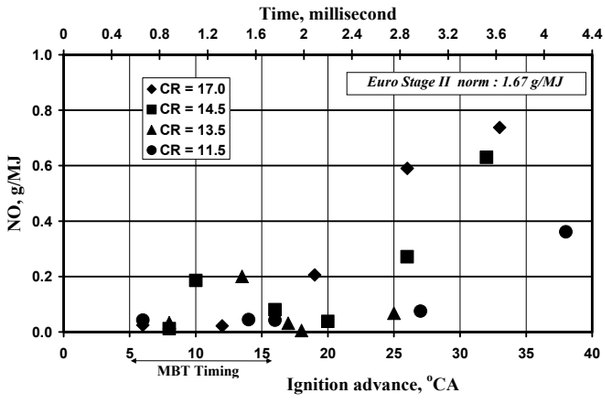


Fig. 6. Variation of NO with Ignition Advance at Various CRs

5.3 Summary of the experimental work

Performance of the engine at higher CR is smooth and it has been established that the engines using producer gas in SI mode at CR up to 17 is feasible. This is obvious from the p-θ curve, which shows a smooth rise in pressure without any pressure oscillations. A shorter duration of combustion has been observed with producer gas fuel, requiring retardation of the ignition timing to achieve MBT. These faster burning cycles are corroborated by low cyclic pressure fluctuations with coefficient of variation ~ 3%. The faster burning process is due to higher flame speed of the fuel - air mixture and this is attributed to the hydrogen content in the gas. The MBT arrived from this study is much retarded than claimed by the earlier researchers. The MBT in the current case are in the range between 6 and 17° CA for CR range between 17 and 11.5 against 30 - 45° CA (for a CR of 11.5 and below) claimed by the earlier researchers. This change in ignition advance in the present study can only be attributed to the improved producer gas composition.

The maximum de-rating in power is observed to be 16.7% in gas mode compared to diesel operations at comparable CR. The extent of de-rating is much lower when compared to any

of the previous studies (Parke et al., 1981; Ramachandra, 1993; Martin et al., 1981). This value matches with a similar kind of de-rating reported (Das & Watson, 1997) with natural gas operation. However, the brake thermal efficiency drops down by 5% compared to normal diesel mode of operation. This is related to excessive heat loss to the coolant at all CRs. The emission in terms of NO is found to be much lower.

6. Modeling of engine processes

The ability to utilize experimental data in new situations and conditions other than those where experiments are conducted is truly enhanced by using mathematical modeling. Modeling is classified as thermodynamic or fluid dynamic either based on energy conversation or on a complete analysis of fluid flow (Heywood, 1988). The thermodynamic models are more popularly known as zero-dimensional, phenomenological or quasi-dimensional models. The fluid-dynamic based models are often multidimensional due to their inherent ability to provide detailed information of the flow field and involves solving of governing equations of flow. Both the approaches are presented here. Initially the zero dimensional modeling results are validated against the experimental results; the limitations are identified and further a three dimensional CFD based modeling results are presented. Both the zero dimensional and three dimensional modeling require certain fuel related properties as input to the model. One among them is the laminar burning velocity (S_L) of a gaseous fuel, which is function of fuel composition, reactant pressure and temperature. Laminar burning velocity for fuel-air mixture can be determined either from experiments or theoretical calculations. The data relating to laminar burning velocity (S_L) of typical producer gas is given in Sec. 4.1

6.1 Zero dimensional modeling

The model comprises of sub-models to simulate the four processes of reciprocating engine cycle namely intake, compression, heat release followed by expansion and exhaust. The various sub-models used in the above simulation are (a) the filling and emptying technique for intake and exhaust processes (Heywood, 1988) as outlined, (b) Eddy Entrainment and Laminar Burn-up (EELB) model (Keck, 1982) for simulation of heat release, and (c) the heat loss due to convection based on Annand's convective heat transfer correlations (Annand, 1963; Baruah, 1986). The flame propagation (or heat release) is modelled as a two-zone model, where a thin wrinkled multi-connected laminar flame separates the burned and the unburned mixture. The EELB model (Keck, 1982) is represented by two equations namely,

$$\frac{dm_b}{dt} = \rho_u A_f S_l + \frac{\mu}{\tau_b} \tag{2a}$$

$$\frac{d\mu}{dt} = \rho_u A_f u_T - \frac{\mu}{\tau_b} \qquad \text{Where} \qquad \mu = \rho_u \ell_T (A_\ell - A_f) \tag{2b}$$

Eq. (2a) represents the mass burn rate, whereas Eq. (2b) represents the rate of change of mass of unburned mixture within the flame front. In these equations, there are two quantities, namely the characteristic speed (u_T) and length (ℓ_T), which could be related to the turbulence parameters namely u' and l_I. Turbulence parameters namely turbulence intensity and length scales are extracted from the CFD results and used as a 0-D model

input. It was further assumed that during combustion, the unburned mixture undergoes isentropic compression sufficiently rapidly for the simple distortion process to occur. These are given as follows:

$$u' = u_0'\left(\rho_u/\rho_0\right)^{1/3} \; ; \; l_I' = l'_{I,0}\left(\rho_u/\rho_0\right)^{-1/3} \tag{3}$$

where ρ_u refers to the density of the unburned gas, ρ_0 refers the state at the start of combustion, u' and u_0' refers to turbulence intensity under reacting and non-reacting conditions respectively, similarly l_I' and $l_{I,0}'$ refers to integral length scale under reacting and non-reacting conditions respectively.

6.1.1 Zero Dimensional modeling results

In these computations, appropriate fuel-air mixture recorded during experiments constituted the input energy (IE). The recycled gas fraction in the total air + fuel mixture was calculated in the gas exchange process of the thermodynamic cycle simulating firing conditions. In the Table 6, Case No. 1 (in italics) corresponding to an ignition advance of 26° CA at CR=17.0 was used as a trial case for choosing the coefficients for the heat loss equation. The computed p-θ curves and their comparison with experimental results are given below.

Case no.	CR	Composition, Vol %			Φ	I*	Ign, °CA	Ign delay, °CA
		H_2	CO	CH_4				
1	*17.0*	*20.8*	*16.2*	*2.0*	*1.10*	*1.70*	*26*	*12*
2	17.0	21.0	18.6	2.0	1.03	1.70	22	9
3	17.0	21.5	16	2.5	1.09	1.69	17	9
4	17.0	2.10	19.2	2.0	1.00	1.69	12	9
5	17.0	20.0	20.0	2.0	1.10	1.73	6	6
6	13.5	20.0	15.0	2.5	1.06	1.62	25	9
7	13.5	20.0	15.0	2.5	1.07	1.63	18	9
8	13.5	20.0	15.7	2.5	1.06	1.63	14	9
9	11.5	18.0	18.0	2.5	1.09	1.63	27	9
10	11.5	21.0	20.0	2.0	1.07	1.70	17	9
11	11.5	19.5	20.0	2.0	1.07	1.66	6	6

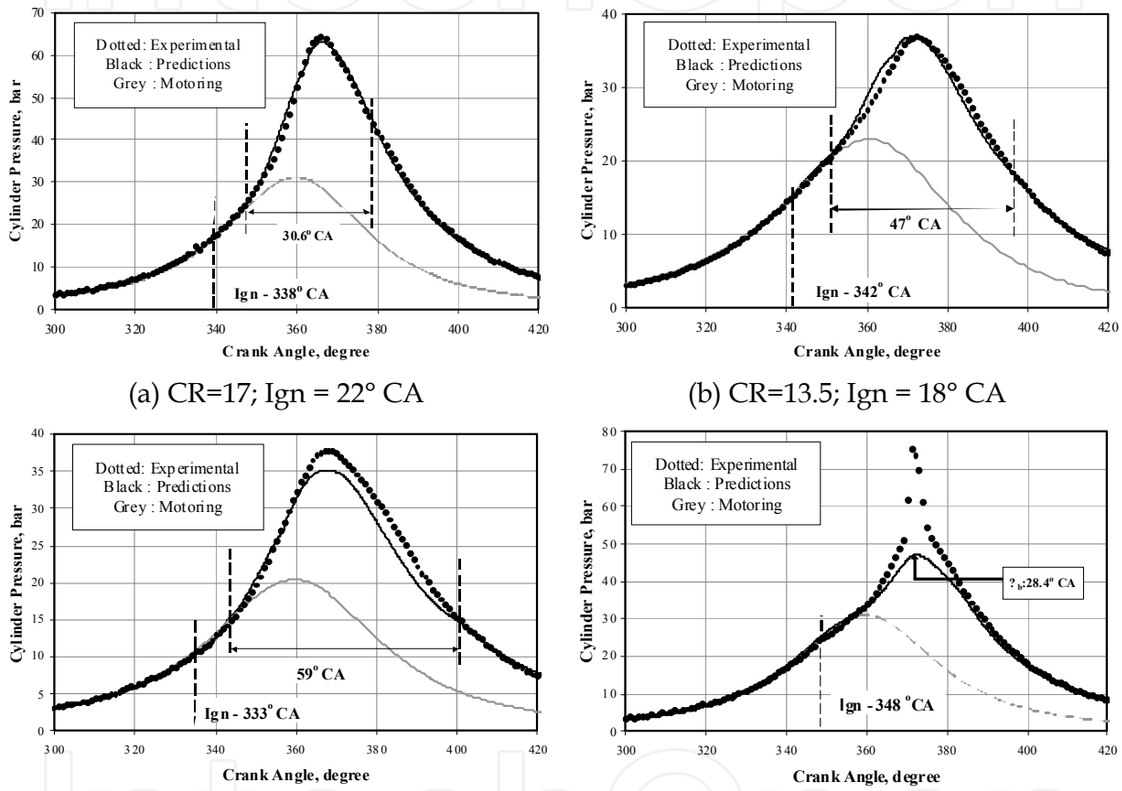
* I=Input Energy/cycle, kJ

Table 6. Principal Parameters of the Test Cases Used in the 0-D Computations

6.1.2 Computational results at advanced ignition setting

The results of five test cases (Case Nos. 1, 2, 6, 7, 9 in Table 6) are discussed here. The ignition settings of these cases are between 18 and 27° CA. All the five cases are computed with the well-observed phenomenon of a spherical flame propagating into the unburned mixture. With the ignition occurring at the pre-set time, a flame kernel forms at the ignition site. During the ignition delay period, the flame kernel is assumed to move vertically downward due to the surrounding turbulent fluid flow. Subsequent to the ignition delay period, the EELB model of flame propagation is invoked wherein a spherical flame is assumed to propagate into the unburned mixture, with continued movement of the flame

due to local fluid velocities. This spherical flame propagation continues till the flame encounters a wall, further the entrained unburned mixture is assumed to burn exponentially. During the quasi-steady flame propagation, typical turbulent burning velocities are of the order of 7-9 m/s (at CR = 17.0) and time scale of the order of 0.5– 0.6 ms during the initial stages of flame propagation, and once the flame reaches the wall, time scale for exponential burning is of the order of 0.8 to 1.0 ms and somewhat similar to the value (0.6 to 1.0 ms) reported (Keck, 1982). The computations one each for every CR is shown in Fig. 7 a - c. The computed results at all CRs matched reasonably well with the experimental data.



(a) CR=17; Ign = 22° CA (b) CR=13.5; Ign = 18° CA

(c) CR=11.5; Ign = 27° CA (d) CR=17; Ign = 12° CA

Fig. 7. p-θ Computation at varied CRs and with different Ignition Advances

6.1.3 Computational results at less advanced ignition setting

The results of six test cases corresponding to less advanced ignition setting (Case Nos. 3, 4, 5, 8, 10, 11 in Table 6) are discussed here. Computations using spherical flame assumption were made for all the six test cases, one test result corresponding to CR=17 at 12° CA ignition advance is shown in Fig. 7 (d). From the figure it is evident that there is deviation in the computed pressures beyond a certain crank angle (CA). At careful look at the experimental curve shows that there is a steep rise in the cylinder pressure. Therefore, at less advanced ignition setting the enhanced fluid dynamics due to reverse squish flow could be modifying the burn rate to such an extent that there is a steep rise in cylinder pressure. The cold flow CFD studies (Sridhar et al., 2004) clearly indicate high velocity jets coming out of

the bowl and reentering the cylinder during reverse squish period. And whenever major part of the combustion occurred during this time, there appears to be abrupt increase in the burn rate leading to steep pressure rise. This effect is observed to be more severe at higher CR of 17 and 13.5 as compared to CR=11.5. This could be true because, the peak reverse squish velocities (without combustion) with CR=17 is of the order of 31 m/s as against 6 m/s for CR=11.5 (Sridhar et al., 2004). Therefore, the deviations in the computed results at CR = 11.5 is lower compared to CR= 17 and 13.5.

Furthermore, the 0-D model is used to estimate the work produced in a completed thermodynamic cycle by integrating the pressure-volume data over a complete cycle resulting in indicated power (IP). At advanced ignition timing, the 0-D model is able to make reasonably good predictions by assuming the conventional spherical flame propagation model. The IP is under-predicted by about 3% for CR=17.0 and 11.5, and between 5 and 8% for the other two cases at CR=13.5. In all the eleven test cases that were discussed, for higher CR of 17 and 13.5 the error in the 0-D prediction is large in around ignition advance of 6 and 12° CA respectively. Whereas, for lower CR = 11.5 the error in 0-D prediction is of the order of 5 – 6%. This under- predication is attributed to the strong complex fluid flow-flame interaction occurring during the reverse squish period, which requires a detailed 3-D CFD modelling to understand the phenomenon. The results of one such study are given in the following section.

6.2 Multi-dimensional modeling

Combustion problems involve strong coupling between chemistry, transport and fluid dynamics. Multi-dimensional turbulent combustion models are expected to simulate turbulent flames and to provide an estimation of mean production or consumption rates of chemical species. They need to be based on known quantities (mean flow characteristics, for example) or on quantities that may be easily modelled or obtained from closed balance equations. Three main types of approaches are; scalar dissipation rate estimation, geometrical analysis, and statistical method (Veynante & Vervisch, 2002). In the geometrical analysis, the flame is described as a geometrical surface. This analysis is generally linked to the assumption of a sufficiently thin flame, viewed as an interface between fresh and burnt gases in premixed combustion. Two formalisms of geometrical analysis are; G-field equation and flame surface density (FSD) concept. The FSD approach is explained below.

6.2.1 Flame surface density model

In this model, the flame is identified as a surface and the flame surface density (Σ) is the available flame area per unit volume. The mean burning rate of an i^{th} specie ($\overline{\dot{\omega}_i}$) is modelled as:

$$\overline{\dot{\omega}_i} = \dot{\Omega}_i \Sigma \tag{4}$$

where $\dot{\Omega}_i$ is the mean local burning rate per unit flame area integrated along the normal direction to the flame surface. The main advantage of this formulation is to decouple the chemical description from the flame/turbulence interaction. The mean consumption rate per unit volume at a point in the flow is determined as the product of flame surface density at that point and the volume consumption rate per unit of flame area, obtained from the

analysis of local strained laminar flamelets. Thus the mean burning rate of an i^{th} species, $\bar{\dot{\omega}}_i$ in a stretched laminar flamelet regime is given as,

$$\bar{\dot{\omega}}_i = \rho_u Y_{u,i} I_0 S_L \Sigma \tag{5}$$

where ρ_u is the density of unburnt reactant mixture ahead of flame front,
$Y_{u,i}$ is the mass fraction of the ith species,
I_0 is the mean stretch factor of stretched laminar flamelet in turbulent mixture,
S_L is the laminar burning velocity of the fuel.
The flame surface density (Σ) is estimated by solution of a balance equation. The balance equation for flame surface density (Σ) can be written as:

$$\frac{\partial \Sigma}{\partial t} + \nabla \cdot (U\Sigma) = \nabla \cdot (\frac{\nu_t}{\sigma_\Sigma} \nabla \Sigma) + S - D \tag{6}$$

where S is the production rate of flame surface density (Σ) by turbulent rate of strain, and D is the annihilation rate of flame surface density by mutual collision. ν_t is the turbulent kinematic viscosity, and σ_Σ is the flame surface turbulent Schmidt number. The above equation is an exact balance equation with unclosed terms, S and D.

Model	***S***	***D***
Cheng model (Cheng et al., 1991)	$\alpha\sigma \frac{\varepsilon}{k} \Sigma$	$\frac{\beta S_L \Sigma^2}{\left(\bar{Y}/Y_0\right)}$
CFM-2 model (Choi & Huh, 1998)	$\alpha \frac{u'}{l_{tc}} \Sigma$	$\frac{\beta S_L \Sigma^2}{\left(\bar{Y}/Y_0\right)\left[1-\left(\bar{Y}/Y_0\right)\right]}$
Modified FSD model (Yarasu, 2009)	$\alpha \frac{u'}{l_t} \Sigma$ where $l_t \geq l_{tw}$	$\frac{\beta S_L \Sigma^2}{\left(\bar{Y}/Y_0\right)\left[1-\left(\bar{Y}/Y_0\right)\right]}$

Table 7. Production term, S and Annihilation, D of flame in Eq. (6)

The main focus of modelling is the production and annihilation terms, S and D. The summary of available closures of S and D, are given in the literature (Veynante & Vervisch, 2002). Formulation of S and D used in present simulations is explained.

- **Production term *S***

The term ***S*** is proportional to Σ in all models as shown in Table 7. It is given as a product of the average rate of strain and the flame surface density. The average rate of strain may be estimated as $1/\tau_t$ from the rate of strain of large energy-containing eddies. The symbol ε represents the dissipation rate of turbulent kinetic energy, k. In CFM-2 model (Choi & Huh, 1998), the average rate of strain is given proportional to $u'$and production term ***S*** is given as:

$$S = \alpha \frac{u'}{t_{tc}} \Sigma \tag{7}$$

where l_{tc} is an arbitrary length scale which was introduced for dimensional consistency. l_{tc} value 1.26 mm was suggested for constant volume combustion in a closed vessel (Choi &

Huh, 1998). Also, it was suggested to combine this constant value with the model tuning constant α. A particular value of l_{tc} will be suitable only for a particular value of turbulent length scale in a closed vessel of isotropic turbulence. If l_{tc} is replaced with turbulent integral length scale l_t and specifying a limiting cut off value near the wall, the model would be suitable for simulation of both the constant volume combustion in a closed vessel and engine combustion of varied turbulent length scales. Hence in the modified FSD model (Yarasu, 2009), production term *S* is used as;

$$S = \alpha \frac{u'}{l_t} \Sigma \quad \text{where} \quad l_t \geq l_{tw} \tag{8}$$

where l_{tw} is cut-off turbulent integral scale near the wall. The limiting value near the wall prevents the unphysical flame generation and acceleration along the wall. The cut-off value l_{tw} to be determined with help of a plot (Yarasu & Paul, 2007) of l_t in the domain or it may also be taken as an average integral length scale of entire domain.

- **Annihilation or Destruction term, D:**

The term D is proportional to Σ^2 in almost all models (see Table 7). This is reasonable, since annihilation occurs due to collision between flame surfaces. In CFM-2 (Choi & Huh, 1998) model, it is given as;

$$D = \beta \frac{S_L}{\left(\bar{Y}/Y_0\right)\left[1-\left(\bar{Y}/Y_0\right)\right]} \Sigma^2 \tag{9}$$

where β is model tuning constant. S_L - Laminar burning velocity, $\bar{Y}$ = mean fuel mass fraction, and Y_0 = fuel mass fraction in the fresh mixtures. The denominator in the D term of Cheng model is $\bar{Y}/Y_0$ (Cheng & Diringer, 1991) while CFM-2 use $\left(\bar{Y}/Y_0\right)\left[1-\left(\bar{Y}/Y_0\right)\right]$.

The EBU model is limiting form of the CFM-2 model for infinitely fast chemistry and steady balance between production and annihilation of flames. Hence, in the present model, the term *D* is taken same as that of CFM-2 model. The predictions of CFM-2 model were tested in constant volume combustion chamber with hydrocarbon flames and the limitations were identified (Choi & Huh, 1998; Yarasu et al., 2005). The modified FSD model was validated for constant volume combustion of producer gas-air mixture with initially induced turbulence. It was observed that there is a delay in development of initial flame kernel (Yarasu, 2009). Once the flame kernel is developed, the combustion rate is predicted well. The delay also depends on initial turbulent intensity in the domain. The delay decreases as the initial turbulent intensity increases. The delay was suitably compensated by offsetting ignition timing in the computations compare to experimental setting by advancing it about 3-4° CA. The modified FSD model predictions for a critical case of CR 17 and varied ignition timing of 26°, 12° and 6° CA are given in the following section.

6.2.2 Engine combustion simulation

CFD simulation of producer gas engine combustion process was carried out using ANSYS-CFX-10 software. The flame surface density (FSD) based combustion models are not available in ANSYS-CFX. Hence, it was implemented in ANSYS-CFX with user FORTRAN code for the source terms in transport equation of Σ, which is Eq.(6). During the

compression and combustion process simulations, structured meshes having 0.04 to 0.1 million cells were used. K-epsilon turbulence model was used for flow simulation. Initial flame kernel was given by providing high flame surface density in a small volume comparable to the spark size at the time of ignition and location. The integral length scales in the domain along the line normal to the cylinder head surface at spark location was plotted in Fig. 8. This graph was used for determining the limiting value of l_{tw} near the wall of the domain, refer Eq (8). The slope of the curve near the wall at point A, about 5 mm away from the wall, is growing steeper. A tangent drawn at point A intersects the ordinate at point B. The cut-off integral length scale value l_{tw} near the wall is the value of l_t at point B which is equal to 3.4 mm for the computational domain considered. The point A was located intuitively. A more scientific method is required to fix the l_{tw} value for a particular domain.

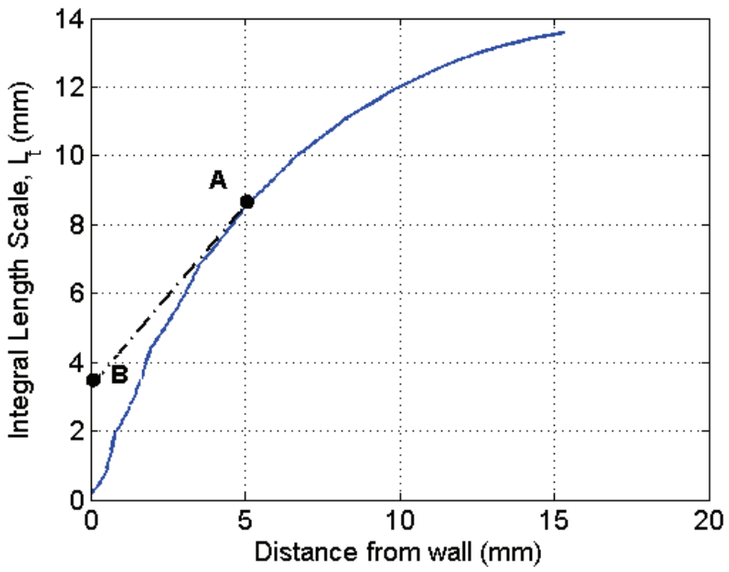
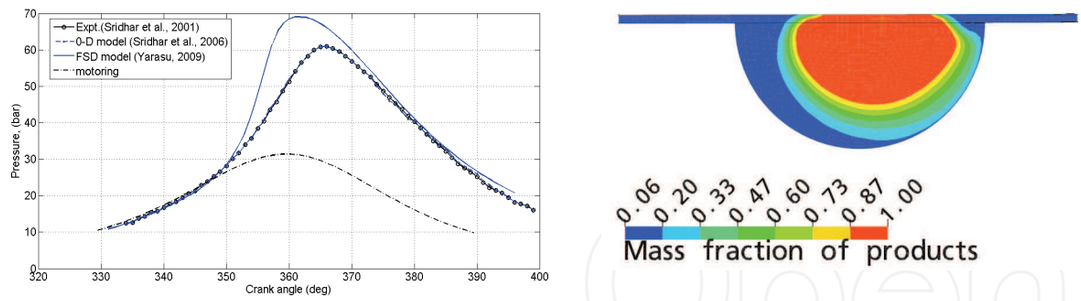


Fig. 8. Integral length scale plot

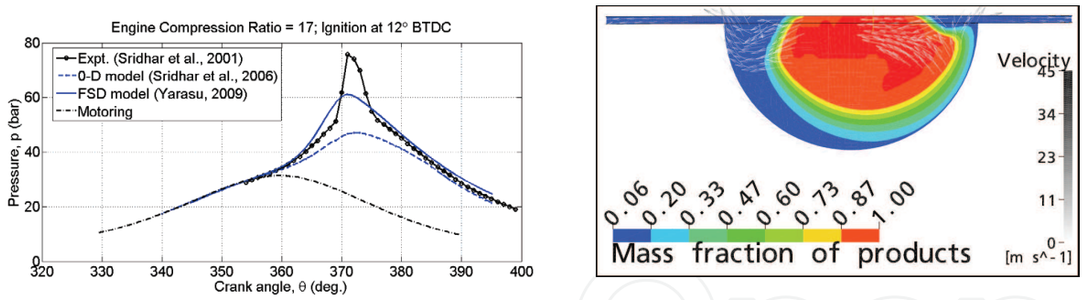
The modified FSD model prediction for a critical case of CR 17 and ignition timings of 26°, 12° and 6° CA BTC were compared below. The progress rate of combustion with different ignition timings was analyzed. The ignition timing in the simulation was advanced by 3-4° CA in order to compensate initial flame kernel development (this was not so with the 0-D modelling). For ignition at 26° BTC case, the simulated (3-D and 0-D) and experimental p-θ values are compared in Fig. 9a. The products mass fraction profile is shown in the Fig. 9b. The flame front was touching bowl walls. The simulated 3-D pressure curve follows the experimental curve up to 351°CA. During the combustion process, the shape of the flame remained very close to the spherical flame front and it was propagating in slightly suppressed turbulent flow field compared to the flow field that prevailed during the motoring operation. Thereafter, the 3-D model pressure values were over-predicted. The reason for over-predicting the pressure value could be due to higher flame generation near the walls, which is related to cut off value of l_{tw} near the wall (Fig.8). It also suggests that l_{tw} value need to be increased with suitable criteria. However, the zero dimensional predictions are much closer to experimental values in this particular case.



(a) (b)

Fig. 9. Results at ignition advance of 26° CA (a) p-θ diagram comparison; (b) Product mass fractions profile at 354° CA

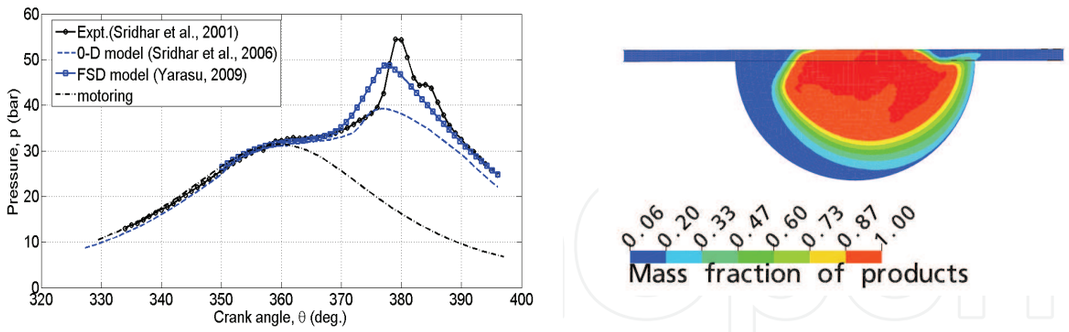
For ignition at 12° BTC case, comparison of the simulated (3-D and 0-D) with the experimental p- θ diagram of the engine is shown in Fig. 10a. The simulated pressure curve follows the experimental curve up to 363° CA. Thereafter, the pressure values were slightly over predicted by FSD model. In this case, the flame approached the bowl walls by 363°CA. The products mass fraction profile is shown in the Fig. 10b. The flame front was touching bowl walls. The burn rate was slightly over-predicted. It also suggests that l_{tw} value need to be increased with suitable criteria. The FSD model under-predicted the peak pressure by 18% (Yarasu, 2009). However, it has the inherent ability to predict the higher burn rate during reverse squish period for this complex case. FSD model predicted pressure values have better matching compared to zero dimensional prediction.



(a) (b)

Fig. 10. Results at ignition advance of 12° CA (a) p-θ diagram comparison; (b) Product mass fractions profile at TC

For the ignition at 6° BTC case, comparison of simulated (3-D and 0-D) and experimental p-θ diagram of the engine is shown in Fig. 11a. The products mass fraction profile is shown in the Fig. 11b when the flame front was touching bowl walls. Predicted pressure values were again, low compared to the experimental values. The simulated pressure curve matched well up to 370° CA. Thereafter, the pressure values were slightly over-predicted by FSD model. The reason could be due to the slight higher burn rate predicted by the model when the flame surface is near the wall. However, the simulated curve still under-predicted the peak pressure by 9%, but there is better match of predicted pressure values of FSD model compared to zero dimensional prediction.



(a) (b)

Fig. 11. Results at ignition advance of 6° CA (a) p-θ diagram comparison; (b) Product mass fractions profile at 370° CA

7. Conclusions

The research findings have broken the compression ratio (CR) barrier and it is shown that the engine runs smoothly at CR of 17:1 without any tendency of knock or auto-ignition. Experiments at varying CRs have established the benefits of operating the engine at higher CR in terms of lower de-rating and better efficiencies. A simplified zero-dimensional model is able to predict the engine cylinder pressure versus time cycle and thereof the power output to reasonable accuracy for certain conditions but under-predicts the peak cylinder pressure at less advanced ignition timing or close to optimum ignition timing, in particular at higher CR. These were attributed to the complex fluid flow interaction, which is not possible to account using zero-dimensional modeling. Therefore, a turbulent combustion model based on flame surface density (FSD) approach with wall correction has been used for combustion simulations. The simulations with FSD model for these test cases are much improved compared to zero dimensional results but still falls short of the experimental results. It is however difficult to identify precise reason for these under-predictions until better understanding prevails on the existing models.

It is further anticipated that the knowledge accrued as a consequence of this research activity would help the gas engine community in better understanding of the complex combustion process using producer gas as the fuel; thereof serve as a basis in identifying the optimum operating conditions and also probably the combustion chamber design.

8. Acknowledgement

The work reported in this chapter is a consolidation of research work carried out by the authors between 1996 and 2009. Even though the research was carried out at different time periods, the authors have made a sincere attempt to present an integrated version of the work. The research work was entirely carried out at Combustion Gasification and Propulsion Laboratory, Indian Institute of Science, Bangalore, India under the supervision of Prof. H.S. Mukunda and Prof. P.J. Paul. The authors sincerely thank them.

9. Notations

A_f , A_l	Spherical flame and Laminar burning area, m²	σ_Σ	flame surface turbulent Schmidt number
l_l , $l'_{l,0}$	Integral length under reacting & non-reacting condition, m	k	turbulent kinetic energy, m²/s²
ℓ_T	Characteristic length, m	ε	dissipation rate of turbulent kinetic energy, m²/s³
m_b	Mass of mixture burned, kg	l_{tc}	arbitrary length scale, mm
p, p_o	Actual cylinder pressure and reference pressure , bar	l_t	turbulent integral length scale, m
S_L	Laminar burning velocity, m/s	l_{tw}	cut-off value of l_t near wall
u' u'_0	Turbulence Intensity under reacting & non-reacting condition, m/s	β	model tuning constant
u_T	Characteristic speed, m/s	$\overline{Y}$	mean fuel mass fraction
ρ_u	Unburned gas density, kg/m³	Y_0	fuel mass fraction in the fresh mixtures
ρ_0	Unburned gas density at the start of combustion, kg/m³	LCV	Lower Calorific Value, MJ/kg
μ	Parametric mass, kg	CA	Crank Angle
τ_b	Characteristic time, sec	TC	Top Dead Centre
Φ	Fuel-air equivalence ratio	BTC	Before Top Dead Centre
Ψ	Recycled gas fraction	θ	Crank Angle
θ	Crank Angle	p	Pressure, bar
Σ	flame surface density, m^{-1}	CR	Compression Ratio
$\dot{\Omega}_i$	mean local burning rate per unit flame area integrated along the normal direction to the flame surface, kg / m² s	τ_t	Turbulent time scale, s
$\overline{\dot{\omega}}_i$	mean local burning rate of ith species per unit volume, kg/m³ s	α	model tuning constant
Y	mass fraction	CR	Compression Ratio
I_0	mean stretch factor	MBT	Minimum Advance for Brake Torque
S	production rate of flame surface density (m^{-1}s^{-1})	IP	Indicated Power, kW
D	Annihilation rate of flame surface density (m^{-1}s^{-1})	BP	Brake Power, kW
ν_t	turbulent kinematic viscosity (m²/s)	IMEP	Indicated Mean Effective Pressure, bar
FSD	Flame Surface Density, m^{-1}	PG	Producer gas

10. References

Annand, W. J. D. (1963). Heat Transfer in the Cylinders of Reciprocating I.C. Engines, Proc. Institution of Mechanical Engineers, Vol. 177, pp. 973-990

Anon, (1986). Wood gas as engine fuel, A Report of the Mechanical Wood Products Branch of FAO Forestry Paper No. 72, FAO of United Nations, Rome

Baruah, P.C. (1986). Combustion and Cycle Calculations in Spark Ignition Engines, in the Thermodynamics and Gas Dynamics of I.C. Engines, Vol. 2, pp. 823-865

Caris, D.F. & Nelson, E.E. (1959). A New Look at High Compression Engines, SAE Transactions, Vol. 67, pp. 112-124

Cheng,W.K.& Diringer, D. J. A. (1991). Numerical modelling of SI engine combustion with a flame sheet model. SAE paper 910268

Choi, C. R. & Huh, K. Y. (1998). Development of coherent flamelet model for a spark-ignited turbulent premixed flame in a closed vessel. Combustion and flame, Vol. 114, pp. 336-348

Das, A. & Watson, H.C. (1997). Development of a Natural Gas Spark Ignition Engine for Optimum Performance, Proc Institution of Mechanical Engineers, Part D, Vol. 211, pp. 361-378

Fleischer, F.; Grosse, W. & Zapf H. (1981). Fuels From Biomass and Their Rational Utilisation in I.C. Engines, Proc International Conference - New Energy Conversion Technologies and Their Commercializations, Vol. 2, pp. 1334-1340

Heywood, J.B. (1988). I.C. Engine Fundamentals, International edition. McGraw-Hill

Kanitkar, S.; Chakravarthy, P.; Paul, P.J. & Mukunda, H.S. (1993). The flame speeds, temperature and limits of flame propagation for producer gas-air mixtures-experimental results. Proc. of 4th meet on Biomass Gasification and combustion, pp. 50-62, Mysore, 6-8th Jan. 1993, Bangalore, India

Keck, C.J. (1982). Turbulent Flame Structure and Speed in Spark Ignition Engines, Proc Ninetieth International Symposium on Combustion, The Combustion Institute, Vol. pp. 1451-1466

KeshavaMurthy, T.V.; Ravi, M.R. & Anjan Ray. (2004). Investigation of burning velocity of laminar premixed producer gas/air mixtures at various pressures and temperatures. Proc. of 17th National and 6th ISHMT/ASME Heat and Mass Transfer Conference, pp. 538-543, IGCAR, Kalpakkam, India.

Martin, J. & Wauters, P. (1981). "Performance of Charcoal Gas I.C. Engines, Proc of International Conference - New Energy Conversion Technologies and Their Commercialization, Vol. 2, pp. 1415-1424

Mukunda, H.S.; Dasappa, S. & Shrinivasa, U. (1993). Open-Top Wood Gasifiers, Renewable Energy - Sources for Fuels and Electricity, Island press, pp. 699-728

Mukunda, H.S.; Paul, P.J.; Dasappa, S.; Shrinivasa, U. & Sharan, H. (1994). Results of an Indo-Swiss Programme For Qualification and Testing of a 300-kW IISc-Dasag Gasifier, Energy for sustainable development, Vol. 4, pp.46-49

Natarajan, J.; Lieuwen, T. & Seitzman, J. (2007). Laminar flame speeds of h2/co mixtures: Effect of co2 dilution, preheat temperature, and pressure. Combustion and flame, Vol. 151, pp. 104-119

Parikh, P.P.; Banerjee, P.K.; Shashikantha & Veerkar, S. (1995). Design Development and Optimisation of a Spark Ignited Producer Gas Engine, Proceedings of XIV National Conference on IC engines and Combustion, Vol. 14, pp. 97-107, Pune, India

Parke, P.P.; Stanley, S.J. & Walawnder, W. (1981). Biomass Producer Gas Fuelling of I.C. Engines, Energy From Biomass and Wastes V, pp. 499 –516, Florida

Parke, P.P. & Clark, S.J. (1981). Biomass Producer Gas Fuelling of IC Engines - Naturally Aspirated and Supercharged Engines, American Society of Agricultural Engineers, Michigan, pp. 1-35

Ramachandra, A. (1993). Performance Studies on a Wood Gas Run IC engine Recent advances in biomass gasification and combustion. Proc. of 4th meet on Biomass Gasification and combustion, pp. 213-218, Bangalore, India

Ratnakishore, V.; Ravi, M.R. & Anjan Ray. (2008). Effect of hydrogen content and dilution on laminar burning velocity and stability characteristics of producer gas air mixtures Int. Journal of Reacting flows, Vol. 2008, 1-8

Shashikantha; Banerjee, P.K.; Khairnar, G.S.; Kamat, P.P. & Parikh, P.P. (1993). Development and Performance Analysis of a 15 kWe Producer Gas Operated SI Engine, Proceedings of 4th National Meet on Biomass Gasification and Combustion, Vol. 4, pp. 219-231 Mysore, India

Shashikantha & Parikh, P.P. (1999). Spark Ignited Producer gas and Dedicated CNG Engine - Technology Development and Experimental Performance, SAE paper, 1999-01-3515 (SP-1482)

Sridhar, G.; Paul, P.J. & Mukunda, H.S. (2001). Biomass Derived Producer Gas as a Reciprocating Engine Fuel – An Experimental Analysis, Biomass & Bioenergy, Vol. 21, pp. 61-72

Sridhar, G. (2003). Experiments and Modeling Studies of Producer Gas based Spark-Ignited Reciprocating Engines. PhD Thesis, Indian Institute of Science, Bangalore, India

Sridhar, G.; Paul, P.J. & Mukunda, H.S. (2004). Simulation of fluid flow in a high compression ratio reciprocating internal combustion engine, Proc. IMechE Vol. 218 Part A: J. Power and Energy, No. 218, pp.403-416

Sridhar, G.; Paul, P.J. & Mukunda, H.S. (2005). Computational studies of the laminar burning velocity of a producer gas and air mixer under typical engine conditions. Proc.IMechE Vol.Part A: Journal of Power and Energy, Vol.219, pp. 195-201

Sridhar, G.; Paul, P.J. & Mukunda, H.S. (2006). Zero-dimensional modelling of a producer gas-based reciprocating engine, Proc. IMechE Vol. 220 Part A: J. Power and Energy, No. 220, pp.923-931

Tatom, J. W.; Colcord, A.R.; Williams, W.M.; Purdy, K.R. & Beinstock, D. (1976). Development of a Prototype System for Pyrolysis of Agricultural and Forestry Wastes into Fuels and Other Products, Prepared for EPA

Veynante, D & Vervisch, L. (2002). Turbulent combustion modeling. Progress in Energy and Combustion Science, Vol. 28, pp.193-266

Yarasu, R. B.; Nadkarni, V. & Paul, P. J. (2005). *Laminar and turbulent burning velocities of premixed hydrocarbon-air flames in closed cubical vessel*. Proc. of 19th NCICEC, Chidambaram, India, pp.335-341

Yarasu, R. B. & Paul, P. J. (2007). *Simulation of Premixed Turbulent Combustion of Producer Gas in S. I. Engine*. Proc. of Int. Conf.&20th NCICEC, Hyderabad, India, pp.714-723

Yarasu, R. B. (2009). Premixed turbulent combustion of Producer gas in closed vessel and engine cylinder. PhD Thesis, Indian Institute of Science, Bangalore, India



Paths to Sustainable Energy
Edited by Dr Artie Ng

ISBN 978-953-307-401-6
Hard cover, 664 pages
Publisher InTech
Published online 30, November, 2010
Published in print edition November, 2010

The world's reliance on existing sources of energy and their associated detrimental impacts on the environment- whether related to poor air or water quality or scarcity, impacts on sensitive ecosystems and forests and land use - have been well documented and articulated over the last three decades. What is needed by the world is a set of credible energy solutions that would lead us to a balance between economic growth and a sustainable environment. This book provides an open platform to establish and share knowledge developed by scholars, scientists and engineers from all over the world about various viable paths to a future of sustainable energy. It has collected a number of intellectually stimulating articles that address issues ranging from public policy formulation to technological innovations for enhancing the development of sustainable energy systems. It will appeal to stakeholders seeking guidance to pursue the paths to sustainable energy.

How to reference
In order to correctly reference this scholarly work, feel free to copy and paste the following:

G. Sridhar and Ravindra Babu Yarasu (2010). Facts about Producer Gas Engine, Paths to Sustainable Energy, Dr Artie Ng (Ed.), ISBN: 978-953-307-401-6, InTech, Available from: http://www.intechopen.com/books/paths-to-sustainable-energy/facts-about-producer-gas-engine

INTECH
open science | open minds

InTech Europe
University Campus STeP Ri
Slavka Krautzeka 83/A
51000 Rijeka, Croatia
Phone: +385 (51) 770 447
Fax: +385 (51) 686 166
www.intechopen.com

InTech China
Unit 405, Office Block, Hotel Equatorial Shanghai
No.65, Yan An Road (West), Shanghai, 200040, China
中国上海市延安西路65号上海国际贵都大饭店办公楼405单元
Phone: +86-21-62489820
Fax: +86-21-62489821

© 2010 The Author(s). Licensee IntechOpen. This chapter is distributed under the terms of the Creative Commons Attribution-NonCommercial-ShareAlike-3.0 License, which permits use, distribution and reproduction for non-commercial purposes, provided the original is properly cited and derivative works building on this content are distributed under the same license.

IntechOpen

IntechOpen